JOURNAL OF CATALYSIS 105, 386–404 (1987)

Characterization and Fourier Transform Infrared Studies of the Effects of TiO_2 Crystal Phases during CO Oxidation on Pt/TiO_2 Catalysts

GERALD S. LANE AND EDUARDO E. WOLF[1]

Department of Chemical Engineering, University of Notre Dame, Notre Dame, Indiana 46556

Received October 28, 1986; revised January 6, 1987

The catalytic oxidation of CO was investigated on Pt/TiO_2 catalysts in an infrared cell reactor to study the influence of strong metal–support interaction effects on oxidation reactions and of using different crystal forms of TiO_2. Catalysts were prepared using rutile and anatase TiO_2 and were characterized by chemisorption, X-ray diffraction, and X-ray photoelectron spectroscopy. Hydrogen reduction at 500°C suppresses CO and H_2 chemisorption and leads to changes in Pt $4f_{7/2}$ electron binding energies for both phases of TiO_2. The anatase catalysts show an infrared absorption band around 2091 cm^{-1} which is assigned to linear-bonded CO; whereas, the rutile catalysts show an absorption doublet for adsorbed CO around 2094 and 2075 cm^{-1} and bands around 1840 cm^{-1} assigned to bridge-bonded CO. Both catalysts show the adsorption of CO_2 as a carbonate-like species which is demonstrated to be adsorbed onto the support. The effects of reduction temperature and of support material on CO oxidation activity were compared through temperature-programmed reaction experiments. The catalysts reduced at 200°C show slightly higher activity and lower ignition temperatures than those reduced at 500°C. The rutile-supported catalysts show much higher CO oxidation activity with lower ignition temperatures; the increased activity is speculated to result from a lower activation energy for oxygen desorption. A morphological model of metal–support interactions involving oxygen transfer from the rutile support is proposed to coexist with the Langmuir–Hinshelwood reaction mechanism.

INTRODUCTION

High surface area supports are used to achieve high dispersion of costly noble metals. In addition, supports can affect the catalytic chemistry of metals deposited onto them. Several experimental studies have demonstrated the presence of interactions between metals and supports. One of the first of these studies by Tauster *et al.* (*1*) tested the support effects of TiO_2-supported catalysts by subjecting the catalysts to a low temperature reduction in H_2 at 200°C (LTR) and to a high temperature reduction in H_2 at 500°C (HTR). After an LTR pretreatment, the catalysts exhibited normal chemisorption, but after an HTR pretreatment the chemisorption of CO and H_2 was severely suppressed. Tauster's work (*1–3*) on anatase TiO_2 clearly defined conditions for obtaining a dependence of CO and H_2 chemisorption on the pretreatment of titanium dioxide-supported group VIII metals, and he coined the term strong metal–support interaction (SMSI) to describe this phenomenon. Studies using transmission electron microscopy (TEM) and X-ray diffraction (XRD) on several metal/metal oxide systems report that the loss of adsorption capacity cannot be attributed to sintering, external poisoning, or metal agglomeration (*1*, *4–6*).

Besides kinetic investigations of various metal/metal oxide systems, a variety of characterization techniques and several probe reactions have been used to investigate SMSI characteristics on model and real catalysts. With the reduced chemisorption capacity after an HTR pretreatment, many studies report the rates of surface-

[1] To whom correspondence should be addressed.

0021-9517/87 $3.00

sensitive reactions (dehydrogenation and hydrogenolysis) to be suppressed (*7–10*). However, the hydrogenation of CO shows similar activity after LTR and HTR pretreatments (*11, 12*). These studies demonstrate that turnover numbers for CO hydrogenation increase after H_2 reduction at 500°C (HTR); the turnover numbers for HTR Pt/TiO_2 catalysts have been reported to be 100 times those for Pt/SiO_2 catalysts (*11*). However, since the support modifies the nature of the active metal of a catalyst showing SMSI characteristics, turnover numbers reflect only a relative measure of catalyst activity. Although several authors have indicated that TiO_2-supported catalysts exhibit enhanced methanation activity, a comparison of catalytic activity on a mass-of-metal basis suggests that TiO_2-supported catalysts exhibit an enhanced methanation rate independent of the absence or presence of SMSI characteristics, and that the enhanced rate is dependent on other properties of TiO_2 when compared to other supports (*12*).

Current studies on model catalysts attribute the reduced adsorption capacity to site blockage. Several groups (*13–17*) propose that site blockage involves a migration of support suboxides (TiO_x) ($1 < x < 2$) onto the overlying metal. Using several surface analysis techniques on model catalysts, Belton *et al.* (*18*) have reported that metal encapsulation and electronic interactions result from the migration of the TiO_x species. To explain the high methanation activity but suppressed CO and H_2 chemisorption, some authors speculate that there are metal-migrated oxide interactions which cause increased methanation activity or create special "superactive" sites (*19, 20*). It has been suggested that suboxide migrants have a direct influence on the surface structure and chemistry of CO on metals supported on TiO_2. Raupp and Dumesic (*21*) report a decrease in the initial CO sticking coefficient for Ni/TiO_2, and in another study, Vannice *et al.* (*22, 23*) report that CO and H_2 heats of adsorption on Pt dispersed on TiO_2 are significantly lower than for Pt dispersed on other supports.

Several X-ray photoelectron spectroscopy (XPS) studies (*24–29*) report small reversible shifts in binding energies between LTR and HTR pretreatments indicating that some electron transfer to the metal clusters is occurring. The presence and magnitude of binding energy shifts are being debated; however, the current consensus indicates that there are structural and electronic components contributing to the SMSI phenomenon.

Infrared studies have been conducted to analyze changes in CO adsorption. While several infrared investigations of SMSI-type catalysts have been reported (*30–38*), no clear understanding has emerged. Tanaka and White studied CO_2 dissociation (*31*) and CO adsorption (*32, 33*) on Pt/TiO_2, while Vannice and co-workers investigated SMSI effects on CO adsorption and hydrogenation on Pt/TiO_2 (*11, 34–36*) and Pd/TiO_2 (*37, 38*). Tanaka and White report a doublet for adsorbed CO at 2094 and 2077 cm^{-1} and bridge-bonded CO bands at 1854 cm^{-1}. Vannice and co-workers report a strong linear CO band for LTR Pt/TiO_2 around 2080 cm^{-1} and a weaker band for HTR catalysts around 2050 cm^{-1}.

While the majority of studies reporting SMSI have focused on hydrogenation and hydrogenolysis, only a few CO oxidation studies on SMSI catalysts have been reported. One study by Böcker and Wicke (*39*) investigated oscillations during catalytic CO oxidation using a Pd/TiO_2 catalyst, but they did not explore the effects of reduction. A second study (*40*) reports rates for CO oxidation on Pt/TiO_2 but also fails to report effects of different reduction temperatures.

The main objective of this study was to identify the catalytic importance of the rutile and anatase crystal phases of TiO_2, a factor that has been overlooked in many investigations. The irreversible phase transformation of anatase to rutile is catalyzed by group VIII metals, H_2 partial pres-

sure, and high temperature; hence, the phase transition could be a contributing factor in the catalytic functionality of titania supports. This paper reports the effects of using either rutile or anatase TiO_2 as a support with Pt as the active metal and carbon monoxide oxidation as the probe reaction. The effects of reduction temperature and of metal–support interactions on the catalytic activity for CO oxidation are also reported. CO oxidation was chosen to test if the reduced CO chemisorption capacity after HTR would reduce the effect of CO inhibition and enhance the overall reaction rate. Chemisorption, XRD, and XPS techniques were used to characterize the catalysts, and the overall reaction rate and adsorbed CO species were monitored during transient Fourier transform infrared (FTIR) experiments.

EXPERIMENTAL

Catalysts

The TiO_2 support material used in this study was Degussa Co. P-25 which is a mixture of approximately 70% anatase and 30% rutile. Since the Degussa material is primarily in the anatase form, it was used without pretreatment as an anatase TiO_2 support. In order to obtain the rutile crystal modification of TiO_2, the Degussa TiO_2 was treated with an 8-hr reduction in flowing H_2 at 800°C prior to impregnation. This transformation provided a means of obtaining supports with the same chemical constituents but different polymorphic forms of TiO_2. The platinum was deposited by incipient wetness impregnation onto both forms of the support with solutions of chloroplatinic acid (Alfa Products) at the desired concentrations to give 5.0 wt% Pt loadings. After impregnation, the catalysts were vacuum dried at room temperature for 8 hr. When the drying was completed, the catalysts were pretreated in four ways. Similar to Tauster's procedure (*1*), one batch of the anatase sample was reduced in flowing H_2 for 2 hr at 200°C (A-LTR) and another batch for 2 hr at 500°C (A-HTR). Since the rutile support has a smaller surface area, the rutile-supported catalysts were first oxidized at 300°C in flowing O_2 for 2 hr because it has been reported that higher dispersions are attained by first oxidizing. Following oxidation, half of the rutile catalyst was reduced in flowing H_2 for 2 hr at 200°C (R-LTR) and the rest for 2 hr at 500°C (R-HTR).

FTIR Studies

The catalyst wafers for the FTIR transmission studies were pressed from approximately 80 mg of catalyst powder using a stainless-steel die with a pressure of 8000 psi (55.2 MPa) and were 17.5 mm in diameter and 0.1 mm thick. The catalyst wafers were placed in a specially designed infrared cell reactor described elsewhere (*41, 42*). The infrared spectra were collected at a resolution of 8 cm^{-1} using a Digilab FTS-15C (FTIR) spectrometer. The details of the FTIR and its adjoining apparatus have been reported previously (*41*); therefore, only a brief description of the special features of this system will follow.

The apparatus is equipped with programmable flow and temperature controllers which permit linear changes in the reactant flow rates or in the reactor temperature. These two modes of transient experiments permit testing a wide range of reaction conditions in a limited number of experiments. During temperature-programmed reaction (TPR) experiments, the temperature is increased quasilinearly and then decreased while keeping the reactant concentrations constant. To obtain an approximate value of the catalyst surface temperature, the reactor is equipped with sensitive Chromel–Alumel foil thermocouples placed in direct contact with the catalyst wafer. The exit CO and CO_2 concentrations were monitored with Beckman 315B and Beckman 865 infrared analyzers, respectively. Continuous measurement of the effluent CO_2 and CO concentrations and the CO surface concentration provided an accurate means of determining a relationship between reac-

tion rate and CO coverage throughout an entire TPR experiment. A series of TPR experiments was performed to obtain ignition (light-off) temperatures at various CO feed concentrations. The experiments were conducted at atmospheric pressure in the infrared cell reactor with a total feed gas flow rate of 200 cm^3/min containing 10 cm^3/min O_2 and various amounts of CO with the balance being N_2.

Catalyst Characterization

Physical and chemical adsorption, XRD, and XPS techniques were used to characterize the catalysts.

(a) *Adsorption.* The BET total surface area of each support was measured prior to impregnation with a Quantachrome QS-8 unit using the flow-adsorption method, described by Nelsen and Eggertsen (*43*), and using N_2 as the adsorbing gas and He as the carrier gas. Selective chemisorption experiments were performed using H_2 (99.999%), CO (99.97%), O_2 (99.99%), CO_2 (99.98%), Ar (99.999%), and He (99.999%) gases from Linde Co. The H_2, Ar, and He were purified by passing them through Alltech Oxytraps, and the H_2, O_2, Ar, and He were further purified by passing them through drierite and 5-Å molecular sieves to remove water. The chemisorption capacities of CO, H_2, and CO_2 were measured at 25 ± 3°C by the pulse-flow technique which has been reviewed by Freel (*44*).

(b) *X-ray diffraction.* A Diano XPG-2 X-ray diffractometer was used with Cu$K\alpha$ radiation (λ = 1.542 Å), a 3° beam slit, and a 0.2° detector slit. The source voltage and amperage were 45 kV and 30 mA, respectively. The scan rate for the survey scans of the catalysts was set at 2°/min with a detector time constant of 1 sec. For the X-ray line broadening calculations, a scan rate of 0.5°/min with a detector time constant of 2.5 sec was used due to the relatively low Pt loading. The XRD samples were wafers prepared by the same procedure as used in making wafers for the infrared cell reactor, but the XRD wafers were thicker and were placed on glass slides.

(c) *X-ray photoelectron spectroscopy.* The XPS analysis was performed at the Amoco Research Center in collaboration with Dr. Theo H. Fleisch. Most of the XPS analysis was performed using a Hewlett-Packard 5950B ESCA spectrometer with monochromated Al$K\alpha$ radiation (energy = 1486.6 eV). This instrument is equipped with *in situ* pretreatment chambers for oxidizing and reducing samples. A flood gun was used to neutralize the effect of charging in the samples. Conduction effects were not relevant because the carbon 1*s* electron binding energy (286.4 eV) and the Ti $2p_{3/2}$ electron binding energy (458.4 eV) were used as references in calibrating the other binding energies. In a second set of experiments, an Mg anode (energy = 1253.6 eV) was used instead of an Al anode to avoid the overlap of the Ti LMM Auger line with the sodium 1*s* line and to clearly identify the presence of sodium impurities. The catalyst powders were exposed to three cycles of oxidation in O_2 at 300°C for 2 hr followed by reduction in H_2 for 2 hr at either 200 or 500°C. After these pretreatments, XPS sample wafers were pressed from approximately 50 mg of catalyst powder while being exposed to air. The samples were also reduced under these same conditions in the pretreatment chamber of the XPS unit to eliminate the effects of the exposure to air.

RESULTS

Catalyst Characterization

(a) *BET area, CO and H_2 chemisorption.* The BET total surface area of the anatase TiO_2 agrees with that reported by Degussa; however, the anatase to rutile transition reduces the total surface area from 51.0 to 10.7 m^2/g as shown in Table 1. Table 1 also summarizes the results of H_2 and CO chemisorption. The platinum dispersion values are lower than those reported by other studies; however, the total metal area and the number of metal surface sites reported

TABLE 1

Carbon Monoxide and Hydrogen Chemisorption on 5.0 wt% Pt/TiO_2 Catalysis

Catalyst	CO/Pt	H/Pt	Average crystallite size			%Rutile/ %anatase
			CO_{ad} (nm)	H^{ad} (nm)	XRD (nm)	
R-LTR	0.125	0.115	9.1	9.9	34.7	32.
R-HTR	0.071	0.035	16.0	32.8	31.4	28.
A-LTR	0.105	0.136	10.8	8.3	12.1	0.58
A-HTR	0.030	0.021	38.2	49.8	11.5	0.59
Rutile TiO_2	BET area			10.7 m^2/g		28.
Anatase TiO_2	BET area			51.0 m^2/g[a]		0.58

[a] 50 ± 15 m^2/g reported by Degussa.

here are higher than those of others because a 5.0 wt% Pt loading was used. The effect of H_2 reduction temperature on adsorption capacities for the anatase catalysts is consistent with other SMSI studies (*1*, *36*). The A-LTR catalyst shows normal chemisorption; whereas, the A-HTR catalyst shows almost no adsorption capacity for either CO or H_2. The adsorption capacity of the HTR rutile-supported catalyst (R-HTR) shows a suppression of H_2 and CO chemisorption when compared to the chemisorption capacity of the R-LTR catalyst, but this suppression is not as severe as observed for the anatase-supported Pt catalysts. The rutile and anatase HTR catalysts regain most of the chemisorption capacities found for each of the LTR catalysts after being oxidized for 2 hr at 300°C in O_2 and reduced again for 2 hr at 200°C in H_2. This reversibility in chemisorption capacity is typically reported for SMSI catalysts.

Estimates of the average size of the Pt crystallites are also summarized in Table 1. These values were calculated assuming a 1 : 1 relationship between CO and Pt and between H and Pt. It is also assumed that the Pt crystallites are hemispherical particles with equal proportions of (111), (110), and (100) crystal planes with a reported value of 1.25×10^{15} Pt surface atoms/cm^2 (*45*). The crystallite size estimates for the LTR-pretreated catalysts are similar for the two chemisorbing gases. However, there are differences in the sizes estimated for the HTR-pretreated catalysts since the calculation is sensitive to the number of surface sites. It appears that the suppression of H_2 chemisorption is more severe than suppression of CO chemisorption after an HTR pretreatment since H_2 requires two adjacent sites to dissociatively adsorb. The estimates of Pt crystallite size on both supports after LTR pretreatments are similar, but after HTR pretreatments the size estimates for the rutile catalyst are less than those of the anatase catalyst suggesting there is a higher degree of chemisorption suppression on the anatase catalysts.

(b) *X-ray diffraction.* The XRD results provide a second means of estimating the average size of the Pt crystallites and are shown in Table 1. Average Pt crystallite sizes were estimated using line broadening of the Pt(111) line, the Scherrer equation (*46*), and a correction for instrumental line broadening. Representative XRD patterns for the rutile samples are shown in Fig. 1; curve a represents the R-HTR catalyst after a 300°C oxidation in O_2 and a 500°C reduc-

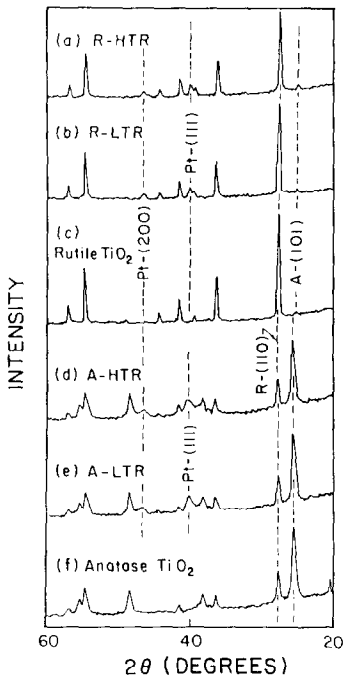

FIG. 1. X-ray diffraction patterns of TiO_2 powder supports and catalysts after pretreatments: (a) 5.0 wt% Pt/TiO_2 R-HTR, (b) 5.0 wt% Pt/TiO_2 R-LTR, (c) rutile TiO_2, (d) 5.0 wt% Pt/TiO_2 A-HTR, (e) 5.0 wt% Pt/TiO_2 A-LTR, and (f) anatase TiO_2.

tion in H_2 and exposure to air, curve b represents the R-LTR catalyst after a 300°C oxidation in O_2 and a 200°C reduction in H_2 and exposure to air, and curve c represents the support. Likewise the anatase samples are depicted in Fig. 1, curves d–f; curve d represents the A-HTR catalyst after a 300°C oxidation in O_2 and a 500°C reduction in H_2 and exposure to air, curve e represents the A-LTR catalyst after a 300°C oxidation in O_2 and a 200°C reduction in H_2 and exposure to air, and curve f represents the support. Two effects are apparent from the XRD estimates of crystallite size shown in Table 1. First, the XRD estimates of the average Pt crystallite size after HTR pretreatment are essentially unchanged from those estimated after LTR pretreatment implying that the suppression of the adsorption capacity cannot be attributed to metal agglomeration. Second, the average crystallite sizes estimated by XRD show that the Pt crystallites on the rutile support are almost three times larger than the crystallites on the anatase support.

A comparison of chemisorption and XRD methods of estimating crystallite size shows some differences between the two supports. The XRD crystallite size estimate for the A-LTR catalyst is similar to the chemisorption estimates. The XRD size estimate for the A-HTR catalyst is similar to that of the A-LTR suggesting that the average Pt crystallite size is independent of pretreatment and that the values estimated by chemisorption are high due to site blockage. However, the XRD estimate of Pt crystallite size on the R-LTR catalyst is much higher than the chemisorption estimates. Two possible explanations of this are that there is a bimodal distribution of Pt crystallites on the rutile support and the smaller crystallites are below the detection limit of XRD or that line broadening estimates of the Pt(111) plane do not accurately represent all the Pt crystallites on the surface. The XRD size estimate for the R-HTR catalyst is similar to the H_2 chemisorption value but remains about the same as the R-LTR catalyst. The discrepancy between crystallite sizes estimated by chemisorption and XRD based on the Pt(111) line could be explained by an effect similar to that suggested for Pd/TiO_2 in which the TiO_x preferentially blocks adsorption on certain crystal planes.

A second application of the XRD results follows the guidelines of Spurr and Myers (*47*). They proposed that the ratio of the maximum intensity of the rutile (110) line to the maximum intensity of the anatase (101) line could be used to estimate the composition of anatase–rutile mixtures; this method has been used by Bond *et al.* (*48*) to estimate the composition of the supporting TiO_2 in their catalysts. The XRD patterns shown in Fig. 1 display the intensities for the rutile (110) and anatase (101) lines that were used to estimate the ratio of the rutile fraction to the anatase fraction which is in-

cluded in Table 1. In addition, the results for the composition of the rutile TiO_2 confirm that the conditions used to induce the phase transition were sufficient to create a predominantly rutile support from the Degussa TiO_2. Although rutile predominates in its form of the support (>96%), the anatase support contains significant amounts of rutile (~35%) as seen in Table 1. (This is pointed out because differences between the crystal modifications presented later could become more pronounced if a rutile-free form of the anatase support had been used.) The X-ray diffraction patterns of the catalysts after their respective pretreatments, shown in Fig. 1, suggest that the supports do not undergo any phase transition during pretreatment or during conditions used in TPR experiments. This is seen in Fig. 1 by comparing the intensity of the rutile (110) line to that of the anatase (101) line for either of the supports (curve c or f) with those of the corresponding catalysts (curves a and b or d and e). When curves a, b, and c or curves d, e, and f are compared, it is apparent that the intensities of the rutile (110) line and the anatase (101) remain unchanged for each TiO_2 phase. The right-most column of Table 1 summarizes the rutile and anatase composition of the supports and supported catalysts.

(c) *Adsorption on titania supports.* As one set of control experiments, selective chemisorption studies using CO, H_2, and CO_2 were performed on the rutile and anatase supports after LTR and HTR pretreatments and are summarized in Table 2. These results indicate that the supports do not provide enough sites for adsorption to occur above the detection limit of the thermal conductivity cell and suggest that no significant chemisorption of CO or H_2 is occurring on the supports. The ability of titania supports to adsorb CO_2 is shown in Table 2 and has been reported previously (*49–51*). The adsorption of CO_2 appears to be directly related to the surface area of the support. The anatase support with almost five times the surface area of the rutile support adsorbs almost five times as much CO_2. The adsorption of CO_2 is supported by infrared results and will be discussed in more detail later.

(d) *X-ray photoelectron spectroscopy.* The two supports and the four catalysts used in this study were analyzed by XPS to determine their surface compositions. Table 3 summarizes normalized surface composition presented as atomic ratios based on surface Ti for the LTR-pretreated catalysts after exposure to air, after an *in situ* H_2 reduction at 200°C for 2 hr, and after an *in situ* H_2 reduction at 500°C for 2 hr. The latter represents the HTR-pretreated catalysts. Table 3 shows that the atomic ratio of Pt to Ti is lower for the anatase-supported catalysts than for the rutile-supported catalysts. This ratio is also lower after an HTR pretreatment than after an LTR pretreatment on both forms of TiO_2. The O/Ti ratio shown in Table 3 does not decrease after HTR pretreatment since the concentration of TiO_x species is small relative to the bulk TiO_2 support. The contribution of the TiO_x

TABLE 2

Adsorption of CO, H_2, and CO_2 on TiO_2 Supports

Support	H_2 reduction temp. (°C)	CO × 10^{-16} (molecule CO/g support)	H_2 × 10^{-16} (molecule H_2/g support)	CO_2 × 10^{-16} (molecule CO_2/g support)
Rutile	200	nd[a]	nd	123.2
Rutile	500	nd	nd	73.7
Anatase	200	nd	nd	366.7
Anatase	500	nd	nd	379.5

[a] nd—below detection limit (< 5 × 10^{16}).

TABLE 3

XPS Surface Composition[a]

Sample	Ti[b]	Pt	O	C	Na	K
R-LTR						
Air exposed	1 (19.3)	0.12	2.64	1.24	0.10	0.08
H_2, 200°C, 2 hr[c]	1 (20.3)	0.089	2.72	0.91	0.09	0.12
H_2, 500°C, 2 hr[c]	1 (22.2)	0.063	2.72	0.49	0.09	0.15
A-LTR						
Air exposed	1 (18.9)	0.042	2.69	1.45	0.06	nd[d]
H_2, 200°C, 2 hr[c]	1 (22.1)	0.038	2.52	0.96	na[e]	nd
H_2, 500°C, 2 hr[c]	1 (22.9)	0.034	2.69	0.61	0.04	nd

[a] Surface composition expressed as atomic ratio based on surface Ti.
[b] Values in parentheses represent relative atomic percentages.
[c] Represents *in situ* reduction at specified conditions.
[d] nd—not detected.
[e] na—not analyzed.

species to the average O/Ti value obtained for the catalyst would be minimal.

Both supports have impurities of sodium and potassium. Since both supports originate from the same initial starting material, Degussa P-25, the increase in the impurities of the rutile samples is likely due to surface segregation during the high temperature phase change. The values presented in Table 3 were acquired using an Al anode, and the Ti LMM Auger line overlaps with the Na 1*s* line. Deconvolution of these lines yields sodium concentrations which are subject to errors as high as a factor of 2. No chlorine was detected for the catalysts indicating that no detectable chlorine was left behind by the chloroplatinic acid precursor. In addition, the XPS results indicate that there is a negative shift in the Pt $4f_{7/2}$ electron binding energy from 70.6 eV after LTR pretreatment to 70.2 eV after HTR pretreatment and from 70.4 eV after LTR pretreatment to 70.0 eV after HTR pretreatment on the rutile and anatase catalysts, respectively. The carbon 1*s* electron binding energy (286.4 eV) was used as a reference in calibrating the Pt $4f_{7/2}$ electron binding energies.

(e) *FTIR studies*. Figure 2 displays representative infrared spectra of adsorbed CO on the four catalysts during exposure to a flowing gas mixture containing 1% CO at 50°C. Reference spectra were taken *in situ* for each catalyst in flowing N_2 and O_2. The sample and reference spectra were taken at a resolution of 8 cm^{-1} and are the result of co-adding 60 scans to improve the signal-to-

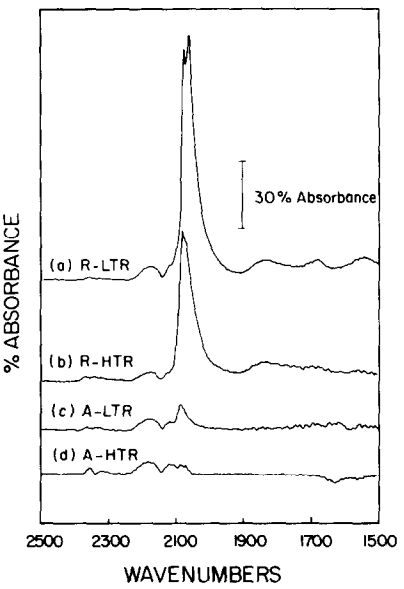

FIG. 2. Infrared spectra of adsorbed CO on 5.0 wt% Pt/TiO_2 (atmospheric pressure, 50°C, 1% CO, 5.0% O_2, balance is N_2, total flow rate of 200 cm^3/min): (a) R-LTR, (b) R-HTR, (c) A-LTR, and (d) A-HTR. Reference spectra were collected at room temperature in flowing O_2 and N_2.

TABLE 4

Observed Band Locations for Pt/TiO_2 Catalyst

Catalyst	CO_2 (gas)	CO (gas)	CO (linear)	CO (bridge)	Reference
R-LTR	2357, 2330	2175, 2110	2087, 2070	1843, 1824	This work
R-HTR	2360, 2325	2177, 2112	2094, 2075	1843, 1836	This work
A-LTR	2359, 2325	2179, 2115	2091	nd[c]	This work
A-HTR	2357, 2320	2179, 2110	~2087	nd	This work
400°C Red[a]			2094, 2077	1854	(*32*)
LTR[b]			2050	1840–1830	(*35*)
HTR[b]			2080	nd	(*35*)

[a] The support is reported by authors as reduced anatase (most likely rutile form due to pretreatment described).

[b] The support is reported by authors as TiO_2 (most likely anatase form due to pretreatment described).

[c] nd—not detected or not reported.

noise ratio. All four spectra show bands for gas phase CO centered around 2175 and 2110 cm^{-1} since the gas phase CO was not subtracted by the references. The spectra also show bands for gas phase CO_2 which result from the reaction of the CO and O_2 at this temperature. The frequencies of infrared band maxima are summarized in Table 4. The interesting features observed in Fig. 2 and Table 4 are the bands for the adsorbed CO species. Spectrum d of Fig. 2 for the A-HTR catalyst shows almost no linear-bonded CO; whereas, spectrum c of Fig. 2 for the A-LTR catalyst shows significant adsorption of linear-bonded CO. This is consistent with the predictions of the chemisorption results for catalysts exhibiting SMSI characteristics. The rutile catalysts show somewhat different behavior; spectra a and b of Fig. 2 show stronger infrared absorbances for the linear-bonded CO species than do the anatase catalysts. Both low and high temperature reduced rutile catalysts exhibit the ability to adsorb IR-active CO. The rutile catalysts also display larger extinction coefficients than the A-LTR and A-HTR catalysts which probably account for the increased absorption of the infrared signal. Attempts to determine extinction coefficients for each catalyst are currently being explored.

In addition to the linear-bonded CO species, bridge-bonded CO species were observed on the rutile catalysts in the range 1860 to 1820 cm^{-1}. Furthermore, the linear-bonded CO on the rutile catalysts shows a doublet. The doublet is more pronounced at a resolution of 2 cm^{-1} indicating that it is a result of two different adspecies and not simply the coadding of a small shoulder onto the strong linear band. The presence of the doublet is dependent on pretreatment; on freshly reduced rutile-supported catalysts the doublet is poorly resolved or not observed. However, as the reaction proceeded in the CO and O_2 atmosphere, the doublet appeared. The doublet is present at both low and high CO surface coverages and hence is assumed not to have a strong surface coverage dependence. Both adsorbed species contributing to the doublet appear active in the oxidation reaction.

The computerized FTIR spectrometer and supporting software were used to follow absorbance band maxima at specified frequencies as a function of time (referred to as spectragrams) during a transient programming experiment. Representative spectragrams from one of the TPR experiments for the R-LTR catalyst are displayed in Fig. 3. As seen in Fig. 3, the transition

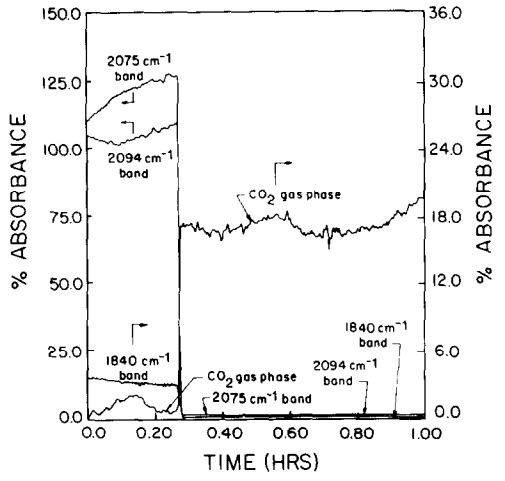

FIG. 3. TPR experiment on a 5.0 wt% Pt/TiO_2 catalyst (R-LTR) with a gas mixture of 15.0 cm^3/min CO, 10.0 cm^3/min O_2 an 175 cm^3/min N_2; spectragram for CO 2094 cm^{-1}, spectragram for CO 2075 cm^{-1}, spectragram for bridge-bonded CO 1840 cm^{-1}, and the spectragram for CO_2 gas phase.

from low to high steady state, characterized by the ignition temperature, gives rise to a drastic decrease in CO surface coverage. Figure 3 displays representative spectragrams for the two bands of the doublet 2090 ± 10 and 2070 ± 10 cm^{-1}, and the bands assigned to the bridge-bonded species 1840 ± 20 cm^{-1}. Figure 3 also displays the spectragram for gas phase CO_2 2350 ± 20 cm^{-1} which shows the increased activity at low CO coverage. Figure 3 indicates that oxygen coverage exceeds that of CO on the Pt surface at high steady state. The spectragrams for all TPR experiments demonstrate similar behavior except for those of the A-HTR catalyst which do not show any change in the linear band because the absorbance level is close to the detection limit of the FTIR.

At a resolution of 8 cm^{-1}, small changes in the frequency of the infrared absorption bands for linear-bonded CO were observed. The linear CO band for both rutile catalysts undergoes a red shift of 5 cm^{-1} as the surface coverage falls when the ignition temperature is approached. These small shifts are consistent with the results of others (*32, 41, 52*). The shifts have been attributed to a change in dipole–dipole interactions with changing CO surface coverage and to an increase in Pt–CO bond strength at low CO coverage.

In addition, Fig. 2 shows infrared bands in the range 1640 to 1320 cm^{-1} for the TiO_2 catalysts. These bands have been assigned to carbonate species adsorbed onto the TiO_2 support (*49–51*). To confirm that these bands are due to adsorption onto the support, wafers of rutile and anatase TiO_2 were placed into the infrared reactor. Figure 4 displays infrared spectra taken on a rutile TiO_2 wafer after exposure to CO_2 and CO, curves a and b, respectively. Spectrum b of Fig. 4 shows no adsorbed species in the range from 2700 to 1700 cm^{-1} indicating that neither linear- nor bridge-bonding of CO was adsorbed above the detection limit of the FTIR on this Pt-free support. However, carbonate-like species adsorbed on the catalysts in the 1640 to 1320 cm^{-1} range of Figs. 2a and 2b were also adsorbed on the rutile support as shown in Fig. 4. The bands assigned to carbonate-like species are more pronounced after exposure to gas phase CO_2 as seen in spectrum a of Fig. 4. The bands in the 2360-cm^{-1} range of spec-

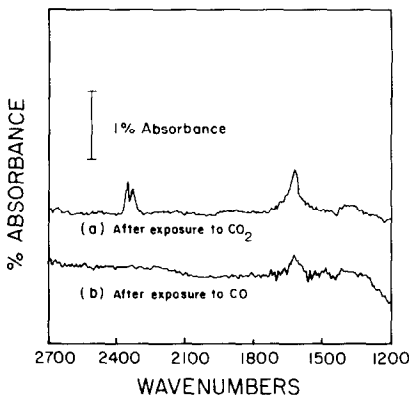

FIG. 4. Infrared spectra of adsorption on Pt-free rutile TiO_2 after exposure to CO_2 and CO: (a) CO_2, (b) CO. Spectra were taken after exposure to gas and degassing in N_2 at room temperature and atmospheric pressure; reference spectra were collected at same conditions in flowing N_2.

trum a are due to desorption of the carbonate-like species at this temperature.

Spectra c and d of Fig. 5 display the infrared spectra taken on an anatase TiO_2 wafer at room temperature after exposure to CO_2 and CO, respectively. Spectrum d indicates that no carbonates nor any CO species adsorb above the detection limit of the FTIR. Spectrum c displays the adsorption of a carbonate-like species and again shows some gas phase CO_2 due to the desorption of the carbonate species. Spectra a and b of Fig. 5 represent spectra taken on the A-LTR catalysts during reaction and show the presence of the carbonate-like species at both low and high CO coverage. The bands of Figs. 4 and 5 are assigned to either unidentate or bidentate carbonate species as reported in the literature (*49, 50*). The carbonate-like species could be removed by degassing in N_2 or by reducing in flowing H_2 at 200°C. Some changes in the magnitude of the absorbance bands in this region, 1800 to 1300 cm^{-1}, are due to temperature effects, and these effects were not subtracted from spectra a and b of Fig. 5.

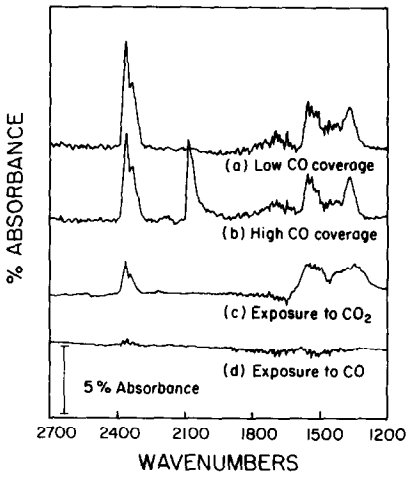

FIG. 5. Infrared spectra on anatase TiO_2: (a) A-LTR catalyst at low CO surface coverage, (b) A-LTR catalyst at high CO surface coverage, (c) support exposed to CO_2, and (d) support exposed to CO. The reference spectra were collected at room temperature under a O_2 and N_2 atmosphere.

Catalyst Activity

TPR experiments were used to monitor CO oxidation activity of a catalyst as a function of temperature in the infrared cell reactor. These experiments provided a means of comparing the CO oxidation activity of the catalysts over a full range of temperatures. The catalytic activity for CO oxidation over a range of feed conditions and temperatures is determined from a series of TPR experiments by varying the feed composition of CO. The experimental observations were confirmed to be reproducible by performing several experiments using different wafers and two different batches of catalysts. Wafers of rutile and anatase TiO_2 were placed into the infrared reactor to serve as control experiments. The results of the TPR experiments on rutile and anatase demonstrate that neither the supports, the stainless-steel reactor walls, the aluminum sample holder, nor the Chromel–Alumel surface thermocouples contribute significantly to the catalyst activity for temperatures up to 300°C. Control experiments on the supports (15 cm^3/min CO, 10 cm^3/min O_2 in 175 cm^3/min N_2 at 310°C) showed rates of 0.02 μmole CO_2 sec^{-1} which were considered negligible since the rate was at most 0.5% of the rate determined in the experiments using the catalysts at these conditions. Since the supports show little activity in these control experiments, the supports do not appear to affect the activity in the absence of Pt.

Figure 6 compares the activity of the four catalysts during the heating portion of two sets of TPR experiments. For a fixed O_2 concentration of 5.0%, Fig. 6a represents an experiment for a feed of 7.5% CO, and Fig. 6b represents an experiment for a feed of 1.0% CO. As shown in this figure, the rutile-supported catalysts exhibit ignition, an abrupt transition from a low steady-state conversion of CO to a high steady-state conversion of CO, at lower temperatures than the anatase-supported catalysts. The ignition temperature is defined as the temperature at which this transition takes

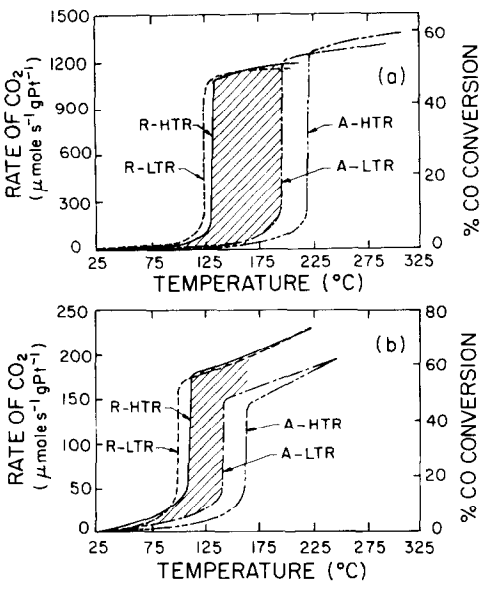

FIG. 6. (a) TPR experiment with a gas mixture of 15.0 cm^3/min CO, 10.0 cm^3/min O_2 and 175 cm^3/min N_2 for 5.0 wt% Pt/TiO_2 on the four types of catalysts. (b) TPR experiment with a gas mixture of 2.0 cm^3/min CO, 10.0 cm^3/min O_2 and 188 cm^3/min N_2 for 5.0 wt% Pt/TiO_2 on the four catalysts, R-LTR, R-HTR, A-LTR, and A-HTR.

place. The differences in ignition temperatures for the rutile and the anatase catalysts are about 75°C. The differences in ignition temperatures due to LTR and HTR pretreatments of the catalysts are about 10 to 20°C indicating that the pretreatment has less of an effect on activity than does the phase of the TiO_2 support. The cross-hatched regions of Fig. 6, between the ignition curves, show regions of increased CO_2 production for the rutile-supported Pt. These regions of higher CO oxidation activity reflect the benefits of using rutile instead of anatase as a support for catalytic CO oxidation.

The lower ignition temperatures of the rutile catalysts represent a more active oxidation catalyst. Table 5 compares rates at 127°C for the experiments displayed in Fig. 6b and a 5.0 wt% Pt/SiO_2 catalyst which has been discussed elsewhere (*53*) and also compares ignition temperatures of these experiments. The rates for the four catalysts are summarized on a mass-of-metal basis and turnover numbers (TONs) based on CO and H_2 chemisorption. The rates based on the mass of Pt, summarized in Table 5, show the same trend as the ignition temperatures—the lower the ignition temperature the more active the catalysts. The TONs of Pt supported on rutile and anatase indicate that the rates per site are higher for the catalysts reduced at 500°C and are consistent with previous work proposing an influence of TiO_x overlayers (*13–17*). The turnover numbers are typical of oxidation reactions which are about 100 times those of CO hydrogenation (*11*).

TABLE 5

Comparison of Catalyst Activity[a]

Catalyst	$\Re_G$[b] (μmole CO_2 sec^{-1} gPt^{-1})	$T_{ignition}$ (°C)	TON × 10^3[c] (molecule CO_2/site/sec)	TON × 10^3[d] (molecule CO_2/site/sec)
R-LTR	182	101	284	309
R-HTR	180	113	495	1003
A-LTR	29	142	54	42
A-HTR	13	165	81	116
5 wt% Pt/SiO_2[e]	45	152	56	nd[f]

[a] Comparison is for a feed of 2 cm^3/min CO and 10 cm^3/min O_2 in 188 cm^3/min N_2.
[b] Global rate at 127°C.
[c] Based on CO chemisorption.
[d] Based on H_2 chemisorption.
[e] Ref. (53).
[f] nd—not determined.

DISCUSSION

TiO_2 Supports

Although the rutile and anatase TiO_2 have the same chemical constituents, they have several structural differences. Among these are morphological differences such as defect concentrations and concentrations of exposed crystal planes and chemical differences such as ionic bond strength, acidity, and electron configurations. The role of each of these differences on activity is not clear, but several differences in the supports are detected by standard characterization techniques.

The lower BET surface area of the rutile support, shown in Table 1, is explained by the crystal structures of rutile and anatase. When the phase transformation takes place, there is a collapse in the crystal structure due to a distortion of the oxygen framework. Most of the Ti^{4+} ions are rearranged by rupturing two of the six Ti–O bonds. The collapse involves a decrease in cell volume of approximately 8% (*54*). Hence, it is not surprising that rutile TiO_2 has a lower surface area than anatase TiO_2. Also, it has been demonstrated that increasing the calcination temperature tends to reduce the BET surface area of rutile and anatase TiO_2 (*55*). For a given calcination temperature, the surface area of anatase TiO_2 is higher than that of rutile TiO_2.

The CO and H_2 chemisorption on the supports, summarized in Table 2, indicates that the supports do not have active sites to adsorb CO or H_2 above the detection limit of the thermal conductivity cell. However, significant quantities of CO_2 were chemisorbed by both phases of titania. Based on the BET area measurements and using reported values for the molecular cross-sectional area of CO_2 (*56*), both supports chemisorb about 0.015 to 0.018 monolayers of CO_2. Anatase TiO_2, the higher surface area support, adsorbs significantly more CO_2 indicating that the CO_2 adsorption capacity is related to the surface area of the support.

Infrared spectra collected for rutile TiO_2, Fig. 4, and for anatase TiO_2, Fig. 5, indicate that after exposure to CO_2 carbonate-like species exist on the surface. These species are in agreement with those reported earlier (*50*). Figures 4 and 5 show significant differences in the absorption bands depending on the crystal phase of TiO_2. Also, the lower wavenumber bands are well defined on the anatase wafer, but they are not as pronounced for the rutile wafer. A probable cause for this difference is the difference in the concentrations of adsorbed CO_2. As shown in Table 2 and mentioned previously, the anatase support can adsorb almost five times as much CO_2, and this higher surface concentration would affect the intensity of these bands.

The activity of the rutile and anatase supports was tested by placing wafers of each into the infrared cell reactor, and they were found to be relatively inactive up to 300°C. This indicates that the supports (free of Pt) do not contribute significantly to the CO oxidation activity in the temperature range used in the TPR experiments (22–300°C). However, several reports have indicated that CO oxidation does occur on TiO_2 at higher temperatures (>325°C) (*57, 58*). To confirm these reports, a set of CO oxidation studies were performed on rutile and anatase TiO_2 in a quartz microreactor (*59*). Consistent with the results of Onishi and Hamamura (*57*), rutile TiO_2 appears to be more active than anatase TiO_2. Onishi and Hamamura (*57*) attribute the difference in CO oxidation activity to a 19 kcal/mole lower activation energy for oxygen desorption from rutile than from anatase. The reaction mechanism involves gas phase or physisorbed CO reacting with oxygen of the support. The oxygen vacancies created by the reaction would be filled by gas phase O_2.

Platinum Morphology

The CO and H_2 chemisorption results, shown in Table 1, agree with what has been

previously reported and are consistent with a model of TiO_x decoration. The anatase catalysts exhibit the behavior of what have been referred to as SMSI catalysts—normal chemisorption after an LTR pretreatment and suppressed chemisorption after an HTR pretreatment. The suppression of adsorption capacity is more pronounced on the anatase-supported Pt catalysts than for the rutile-supported catalysts. This suggests that the degree of site blockage by TiO_x after an HTR pretreatment is less severe for rutile-supported catalysts than for anatase-supported catalysts. The rutile catalysts appear to alter the mechanism for site blockage. Most likely this alteration is merely a physical one. The surface compositions, determined by XPS and shown in Table 3, indicate that the rutile catalysts have a larger number of Pt surface sites relative to the number of Ti surface sites when compared to the anatase-supported catalysts. Since the surface area of the rutile TiO_2 is less than the anatase TiO_2, the formation of TiO_x on rutile is expected to be reduced. In addition, the XRD results show that the Pt crystallites are much larger on the rutile support than on the anatase support. These larger Pt clusters would hinder the migration of TiO_x onto the Pt for the rutile catalysts. Thus, it appears from the chemisorption results for the rutile and anatase catalysts that the SMSI effect of overlayers is more pronounced for smaller crystallites.

The XPS results of surface composition confirm what is predicated by the surface area, XRD, and chemisorption studies; that is, more surface Pt is detected on the rutile samples because of their lower surface areas and larger Pt crystallites. The atomic ratios of Pt to Ti, shown in Table 3, indicate that the surface Pt decreases relative to the surface Ti after an HTR pretreatment. The rutile catalyst shows a decrease in the Pt/Ti ratio from 0.089 for the 200°C reduced to 0.063 for the 500°C reduced surface. The anatase catalyst exhibits a decrease from 0.038 to 0.034. This decrease in surface Pt can be attributed to coverage by TiO_x as has been proposed by others (*13–18*). The findings presented here indicate that this suboxide migration occurs on both forms of TiO_2. Accompanying the reduction in the surface Pt/Ti ratio, there is a 0.4 eV negative shift in the Pt $4f_{7/2}$ electron binding energy for the catalysts supported on both forms of the TiO_2 after an HTR pretreatment. An *in situ* HTR pretreatment appears to cause a 0.8 eV negative shift from that of metallic Pt, and an *in situ* LTR pretreatment about a 0.3 to 0.5 eV shift from metallic Pt. Several groups have suggested that negative shifts in electron binding energy indicate that some electronic interaction is occurring between the Pt and the TiO_x overlayers. If this is the case, both catalysts demonstrate a slight electronic interaction between the Pt and TiO_2 or TiO_x after a 200°C reduction in H_2 and an increase in this interaction after a 500°C reduction in H_2. It appears that the presence of TiO_x or TiO_2 in either the rutile or anatase form is capable of inducing some electronic interaction with Pt. This interaction is greater on the anatase-supported catalysts; however, the presence of this so-called electronic interaction (negative shift in binding energy) does not appear to greatly enhance CO oxidation activity. The R-LTR catalyst which shows the smallest change in electron binding energy has the best activity. Thus, it appears that if the shifts in electron binding energies have any effect on activity it is not apparent in these ignition temperature studies. The impact of electronic interactions for catalysts with Pt supported on both forms of TiO_2 is currently being further investigated using CO hydrogenation as the probe reaction.

The infrared results presented here help to clarify surface species reported by others. The SMSI (A-HTR) catalyst, Fig. 2 spectrum d, shows minimal existence of any adsorbed CO species (at the detection limit of the FTIR) and is in agreement with the results of Vannice and co-workers (*11, 34, 35*). The existence of a strong linear

band on the A-LTR catalyst, Fig. 2 spectrum c, is also consistent with Vannice's results. Since Vannice and co-workers do not mention any special treatment of their support, the support is assumed to be in the anatase form. Tanaka and White (*32, 33*) refer to their support as reduced anatase, but they do not present XRD results to confirm which form of TiO_2 was used. Based on the infrared results presented here, the support used by Tanaka and White is most likely in the rutile form; the major reason is that their pretreatment of the TiO_2 prior to impregnation was similar to that used in this study to induce the phase transformation. Following this assumption, it is not surprising that their infrared data closely resemble those presented here for the rutile TiO_2 support, Fig. 2 spectra a and b. Tanaka and White's results for TiO_2-supported catalysts that are reduced at 400°C show the appearance of a doublet in the region for linear-bonded CO. The results of this study indicate that the infrared results of Vannice and co-workers and Tanaka and White differ because they used the two different TiO_2 crystal modifications as supports. The infrared spectra for linear-bonded CO on anatase-supported catalysts reported here and by Vannice and co-workers are similar to the single band commonly reported for SiO_2-supported Pt. The doublet reported here and by Tanaka and White is felt to represent CO adsorbed on rutile-supported Pt. Table 4 summarizes the frequencies of the infrared bands and shows consistency in the three sets of infrared data.

The observed doublet is not a unique property of rutile TiO_2-supported catalysts. Almost as many explanations for the doublet have been proposed as there have been reports of the doublet. For Pt/Cab–O–Sil catalysts, Bartók and Sárkány (*60, 61*) attribute the CO doublet to adsorption on Pt sites with different Miller indices. They assign the lower wavenumber band of the doublet to Pt sites having low surface coordination and refer to it as desorptive CO. On the other hand for Pt/Al_2O_3, Barshad *et al.* (*62*) assign the lower wavenumber band, 2070 cm^{-1}, to linear-bonded CO and assign the higher wavenumber band, 2090 cm^{-1}, to CO adsorbed on a platinum atom sharing an oxygen with a coordination number of +1. For Pt/TiO_2, Tanaka and White (*32*) assign the 2094-cm^{-1} absorption band to CO on Pt terrace sites and the 2077-cm^{-1} absorption band to CO on Pt step sites. Terrace and step sites have been shown to have small charge differences and could account for different binding energies (*63*).

These reports suggest that in order to have a doublet two types of sites must exist. Accordingly, one can speculate that the surface of the supporting rutile in this study must be able to enhance the development of two such sites which allows the doublet to develop on the rutile-supported catalysts and not on the anatase-supported catalysts. Since the rutile and anatase crystal structures have different proportions of exposed crystal planes, the planes exposed for the rutile TiO_2 seem to exhibit the proper environment for developing the Pt surface sites needed for the doublet. Since the resolution of the doublet was poor for freshly reduced samples, reduction also appears to hamper the formation of these Pt surface sites. This suggests that the overall crystal morphology is being affected by the reactant gases.

The infrared results presented here suggest that metal–support interactions could have weakened the Pt–CO bond because of the higher wavenumber location of the linear bonds. CO adsorption on Pt supported on SiO_2 has been shown to exhibit its linear band around 2070 cm^{-1} (*41, 42*); whereas, linear-bonded CO on Pt/TiO_2 appears around 2090 cm^{-1}. These values suggest that the Pt–CO bond is stronger when the metal is supported on SiO_2 than on TiO_2. Adsorbed CO appears around 2094 and 2091 cm^{-1} on the rutile and anatase TiO_2 indicating that the Pt–CO bond is about the same strength on both of these supported catalysts. Hence, the absoption frequencies of adsorbed CO do not explain the higher

CO oxidation activity observed for the rutile-supported catalyst.

Akubuiro and Verykios (*40*) report that the activity for Pt-catalyzed CO oxidation is a strong function of the support which is consistent with what is reported here. The activities, compared in Table 5 and in Fig. 6, are found to be dependent on the phase of TiO_2. Ignition temperatures have been reported (*53*) to be almost independent of heat and mass transfer limitations and are basically a function of the competitive adsorption of CO and O_2. A low ignition temperature represents high activity for CO oxidation, and a high ignition temperature represents low activity. Using this as a basis, the A-HTR catalyst has the poorest activity of the catalysts compared. Even with its blocked chemisorption sites, the CO oxidation activity of the A-HTR catalyst is similar to those of the A-LTR and Pt/SiO_2 catalysts which have three to five times as many surface sites. The CO oxidation results for the anatase catalysts show the anomaly reported for CO hydrogenation; the global rate is not suppressed, even though the number of surface sites for SMSI catalysts has decreased as determined by chemisorption measurements. Table 5 compares the activities of the catalysts and indicates two features. The first feature is a small effect on activity by reducing the catalysts at different temperatures. The true magnitude of this effect is difficult to distinguish, because HTR catalysts are not in a well-defined state under CO oxidation conditions since the catalysts regain their chemisorption capacity under oxidizing conditions. To minimize the effects of this problem, activities are only reported up to the ignition point where temperature and time-on-stream are as small as possible. Table 5 shows the large impact on CO oxidation activity that results from using different crystal phases of TiO_2.

Although different crystal modifications are not commonly reported to have this effect on CO oxidation activity, the rutile catalysts exhibit higher activity at this temperature whether they are compared on a basis of global rates, ignition temperatures, or TONs. Differences in activity of rutile and anatase TiO_2 have been demonstrated in other reaction systems. Anatase TiO_2 has been shown to be a better support for the oxidation of *ortho*-xylene to phthalic anhydride (*64*); whereas, rutile-type structures have been shown to exhibit better activity in photocatalysis applications (*32*) and better activity/selectivity in allylic oxidation (*65*). In addition, a recent study of vanadium pentoxide shows that the CO oxidation rate strongly depends on the grain morphology. The higher activity was attributed to morphologies with a higher number of defects (*66*).

A second possibility is the role of the different morphologies of decorating species on rutile- and anatase-supported Pt catalysts. The presence of TiO_x overlayers has been identified as blocking sites for CO and H_2 adsorption. As in CO hydrogenation, the activity for CO oxidation is not significantly affected by pretreatment. Several authors have speculated that these overlayers suppress adsorption on plain crystal surfaces which are not catalytically active but do not suppress adsorption on steps and kinks where active sites are located. This is adequate in explaining the differences between LTR- and HTR-pretreated catalysts. However, it fails to explain the differences between the rutile and anatase catalysts because the anatase catalysts have smaller Pt crystallites, and steps and kinks should be more abundant in small particles. The average size of Pt crystallites has been shown to influence activity for oxidation reactions (*67*). Thus, the difference in the size of Pt crystallites on the rutile and anatase catalysts could affect their activity; however, this earlier report indicates that the global rate is reduced by having larger crystallites, and this is the reverse trend to that observed for the rates summarized in Table 5. The influence of particle size on CO oxidation activity is small relative to the differ-

ences observed between the rutile- and anatase-supported catalysts.

Speculations of altered CO chemistry have arisen in CO hydrogenation studies and would also affect CO oxidation. The mechanism of CO oxidation involves a displacement of CO from the active metal. Thus, any weakening of the Pt–CO bond by metal–support interactions should result in increased activity. Speculations of altered CO chemistry are supported by evidence of a decreased CO sticking coefficient (*21*) and by lowered CO and H_2 heats of adsorption (*22, 23*) for some metals supported on TiO_2. However, evidence suggests that these observations cannot be extrapolated to all group VIII metals supported on TiO_2. From the literature, it appears that titania surface species, TiO_x, block the adsorption on strongly bound sites, hence enhancing adsorption onto more weakly bound sites. The possibility of altered CO chemistry is being examined at this time, and the investigation is concentrating on altered CO desorption rates because of the lower ignition temperatures determined by the TPR experiments.

Pt–TiO_2 Interfaces

The possibility of special active sites at metal-migrated oxide interfaces has been proposed by several groups to explain high CO methanation activity (*19, 20*). These sites have been suggested to be "superactive" and account for high turnover rates on a very limited number of sites for HTR catalysts. A similar explanation to this could account for the high activity on HTR-pretreated catalysts for CO oxidation. These special active sites at Pt–TiO_x interfaces would have to be more abundant on the rutile-supported catalysts to account for their higher activity. The active sites would have high TONs for CO hydrogenation as reported in other studies (*19, 20*) and for CO oxidation as reported in this study.

Alternatively, the transfer of oxygen from the support to an active center for CO would also account for the higher activity of the rutile-supported catalysts. High temperature CO oxidation on rutile TiO_2 has been shown to be more active than on anatase TiO_2 because of a lower activation energy for oxygen desorption from the support (*57*). Thus, a possibility is that in the presence of Pt, the rutile-TiO_2 support acts as an oxygen source and provides a means for oxygen transfer similar to what has been suggested for Pt/CeO_2 catalysts (*68*). The support's surface oxygen or oxygen of the TiO_x overlayers could react with CO adsorbed onto Pt. The rutile support tends to give up its oxygen more freely, and oxygen transfer to an active site of adsorbed CO would reduce CO inhibition and increase activity. A suggested model, displayed in Fig. 7, shows a schematic of a possible means of oxygen transfer with the rutile TiO_2 participating in a redox cycle. This mechanism could coexist with the typical Langmuir–Hinshelwood mechanism of adsorbed CO and adsorbed oxygen reacting. Since anatase TiO_2 has a 19 kcal/mole higher activation energy for oxygen desorption from the support, the activity of rutile-supported catalysts would be increased more by this effect than the activity of anatase-supported catalysts. At this point, the role of an oxygen transfer mechanism is not clear and only speculative; however, it would account for the higher activity of the rutile-supported Pt for CO oxidation.

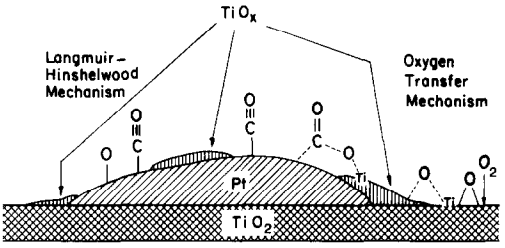

FIG. 7. Schematic of proposed mechanism on the surface of rutile catalysts in which the support is an oxygen source.

SUMMARY

The results show that suppressed CO and H_2 chemisorption, attributed to SMSI, can

be induced on rutile and anatase phases of TiO_2. The decrease in chemisorption capacity is consistent with the model of site blockage by TiO_x. The rutile catalysts do not show as severe a suppression in adsorption capacity, but this is attributed to their larger Pt crystallites and their lower surface area. A higher surface Pt/Ti ratio for the rutile catalysts suggests that it is more difficult for the TiO_x species to migrate onto the Pt when supported on rutile TiO_2. Also, the infrared results clarify the differences in results presented previously. A high temperature (500°C) reduced anatase-supported catalyst shows little IR-active CO adsorption. A low temperature (200°C) reduced anatase-supported catalyst exhibits a single linear-bonded CO band around 2091 cm^{-1}. Rutile-supported Pt catalysts exhibit a doublet in the range of the linear-bonded CO species after reduction at both temperatures. The resolution of the doublet was poor on freshly reduced samples, but treatment under the reaction conditions in CO and O_2 promoted the formation of the doublet, 2094 and 2075 cm^{-1}. In addition the rutile catalysts show bridge-bonded CO bands, around 1840 cm^{-1}, which were active for CO oxidation. The infrared results also suggest that linear-bonded CO is more weakly held to the Pt supported on TiO_2 than to the Pt supported on SiO_2. The shifts in Pt $4f_{7/2}$ electron binding energy suggest that electronic interactions are present on both forms of supporting TiO_2. The degree of shifting relative to metallic Pt is greater for the catalysts supported on anatase and also after HTR pretreatments.

The high temperature reduced (500°C) catalysts do not show a drastic suppression in activity for CO oxidation, even though the adsorption capacity is much lower than the low temperature reduced (200°C) catalysts. Hence, little difference is noted in the rates for the two reduction temperatures. A dramatic change in CO oxidation activity is observed when using rutile TiO_2 as compared to using anatase TiO_2. Regions of enhanced activity and 75°C lower ignition temperatures are observed for the rutile-supported catalysts. Thus, the crystalline form of the support plays a dominant role in determining the activity for CO oxidation; whereas, the reduction temperature plays only a minor role. The reason the rutile catalyst shows a higher CO oxidation activity is not clear, but speculation of an oxygen transfer mechanism from the support is presented. After low or high temperature reduction, the rutile-supported Pt catalysts exhibit greater CO oxidation activity than when Pt is supported on SiO_2 or anatase TiO_2 catalysts; hence, further investigation of rutile as a support and use of this type of catalyst for low temperature catalytic oxidation is warranted.

ACKNOWLEDGMENTS

The authors thank Dr. Theo H. Fleisch and C. M. Willey at the Amoco Research Center for conducting the XPS work for this study. The authors gratefully acknowledge the National Science Foundation for providing partial financial support for this work through NSF Grants CPE-8405900 and CBT-8603033.

REFERENCES

1. Tauster, S. J., Fung, S. C., and Garten, R. L., *J. Amer. Chem. Soc.* **100,** 170 (1978).
2. Tauster, S. J., and Fung, S. C., *J. Catal.* **55,** 29 (1978).
3. Tauster, S. J., Fung, S. C., Baker, R. T. K., and Horsley, J. A., *Science* **211,** 1121 (1981).
4. Baker, R. T. K., Prestridge, E. B., and Garten, R. L., *J. Catal.* **56,** 390 (1979).
5. Baker, R. T. K., Prestridge, E. B., and Garten, R. L., *J. Catal.* **59,** 293 (1979).
6. Baker, R. T. K., Prestridge, E. B., and Murrell, L. L., *J. Catal.* **79,** 348 (1983).
7. Mériaudeau, P., Ellestad, O. H., Dufaux, M., and Naccache, C., *J. Catal.* **75,** 243 (1982).
8. Resasco, D. E., and Haller, G. L., *in* "Studies in Surface Science and Catalysis" (B. Imelik *et al.*, Eds.), Vol. 11, p. 105. Elsevier, New York, 1982.
9. Pande, N. K., and Bell, A. T., *J. Catal.* **97,** 137 (1986).
10. Bracey, J. D., and Burch, R., *J. Catal.* **86,** 384 (1984).
11. Vannice, M. A., and Twu, C. C., *J. Catal.* **82,** 213 (1983).
12. Fang, S.-M., White, J. M., Campione, T. J., and Ekerdt, J. G., *J. Catal.* **96,** 491 (1985).
13. Simoens, A. J., Baker, R. T. K., Dwyer, D. J.,

Lund, C. R. F., and Madon, R. J., *J. Catal.* **86,** 359 (1984).
14. Baker, R. T. K., Prestridge, E. B., and McVicker, G. B., *J. Catal.* **89,** 422 (1984).
15. Takatani, S., and Chung, Y.-W., *J. Catal.* **90,** 75 (1984).
16. Jiang, X.-Z., Stevenson, S. A., and Dumesic, J. A., *J. Catal.* **91,** 11 (1985).
17. Demmin, R. A., Ko, C. S., and Gorte, R. J., *J. Phys. Chem.* **89,** 1151 (1985).
18. Belton, D. N., Sun, Y.-M., White, J. M., *J. Phys. Chem.* **88,** 5172 (1984).
19. Burch, R., and Flambard, A. R., *J. Catal.* **78,** 389 (1982).
20. Vannice, M. A., and Sudhakar, C., *J. Phys. Chem.* **88,** 2429 (1984).
21. Raupp, G. B., and Dumesic, J. A., *J. Catal.* **95,** 587 (1985).
22. Vannice, M. A., Hasselbring, L. C., and Sen, B., *J. Catal.* **97,** 66 (1986).
23. Vannice, M. A., Hasselbring, L. C., and Sen, B., *J. Catal.* **95,** 57 (1985).
24. Huizinga, T., Van't Blik, H. F. J., Vis, J. C., and Prins, R., *Surf. Sci.* **135,** 580 (1983).
25. Chien, S.-H., Shelimov, B. N., Resasco, D. E., Lee, E. H., and Haller, G. L., *J. Catal.* **77,** 301 (1982).
26. Sexton, B. A., Hughes, A. E., and Foger, K., *J. Catal.* **77,** 85 (1982).
27. Fung, S. C., *J. Catal.* **76,** 225 (1982).
28. Belton, D. N., Sun, Y.-M., White, J. M., *J. Phys. Chem.* **88,** 1690 (1984).
29. Kao, C. C., Tsai, S. C., Bahl, M. K., and Chung, Y. W., *Surf. Sci.* **95,** 1 (1980).
30. Jiehan, H., Zupei, H., Yongze, S., and Hongli, W., *in* "Studies in Surface Science and Catalysis" (G. M. Pajonk, S. J. Teichner, and J. E. Germain, Eds.), Vol. 17, p. 53. Elsevier, New York, 1983.
31. Tanaka, K., and White, J. M., *J. Phys. Chem.* **86,** 3977 (1982).
32. Tanaka, K., and White, J. M., *J. Catal.* **79,** 81 (1983).
33. Tanaka, K., and White, J. M., *J. Phys. Chem.* **86,** 4708 (1982).
34. Vannice, M. A., and Twu, C. C., *J. Chem. Phys.* **75,** 12 (1981).
35. Vannice, M. A., Twu, C. C., and Moon, S. H., *J. Catal.* **79,** 70 (1983).
36. Vannice, M. A., Twu, C. C., and Moon, S. H., *J. Phys. Chem.* **75,** 12 (1981).
37. Vannice, M. A., Wang, S.-Y., and Moon, S. H., *J. Catal.* **71,** 152 (1981).
38. Wang, S.-Y., Moon, S. H., and Vannice, M. A., *J. Catal.* **71,** 167 (1981).
39. Böcker, D., and Wicke, E., *Ber. Bunsen-Ges. Phys. Chem.* **89,** 629 (1985).
40. Akubuiro, E. C., and Verykios, X. E., *Appl. Catal.* **14,** 215 (1985).
41. Kaul, D. J., and Wolf, E. E., *J. Catal.* **89,** 348 (1984).
42. Kaul, D. J., and Wolf, E. E., *J. Catal.* **91,** 216 (1985).
43. Nelsen, F. M., and Eggertsen, F. T., *Anal. Chem.* **30,** 1387 (1958).
44. Freel, J., *J. Catal.* **25,** 130 (1972).
45. Scholten, J. J. F., Pijpers, A. P., and Hustings, A. M. L., *Catal. Rev.–Sci. Eng.* **27,** 151 (1985).
46. Cullity, B. D., "Elements of X-Ray Diffraction." Addison–Wesley, Reading, MA, 1978.
47. Spurr, R. A., and Myers, H., *Anal. Chem.* **29,** 760 (1957).
48. Bond, G. C., Sárkány, A. J., and Parfitt, G. D., *J. Catal.* **57,** 476 (1979).
49. O'Neill, C. E., and Yates, D. J. C., *Spectrochim. Acta* **17,** 953 (1961).
50. Rethwisch, D. G., and Dumesic, J. A., *Langmuir* **2,** 73 (1986).
51. Little, L. H., "Infrared Spectra of Adsorbed Species." Academic Press, New York, 1966.
52. Haaland, D. M., and Williams, F. L., *J. Catal.* **76,** 450 (1982).
53. Kaul, D. J., PhD dissertation, University of Notre Dame, 1985.
54. Shannon, R. D., *J. Appl. Phys.* **35,** 3414 (1964).
55. Kikuchi, E., Nomura, H., Matsumoto, M., and Morita, Y., *Pan–Pac. Synfuels Conf.* **1,** 216 (1982).
56. Kodera, K., and Onishi, Y., *Bull. Chem. Soc. Japan* **33,** 338 (1960).
57. Onishi, Y., and Hamamura, T., *Bull. Chem. Soc. Japan* **43,** 996 (1970).
58. Mikhailova, I. L., Sazonova, I. S., and Keier, N. P., *Kinet. Katal.* **6,** 704 (1965).
59. Lane, G. S., and Wolf, E. E., unpublished results.
60. Bartók, M., Sárkány, J., and Sitkei, A., *J. Catal.* **72,** 236 (1981).
61. Sárkány, J., and Bartók, M., *J. Catal.* **92,** 388 (1985).
62. Barshad, Y., Zhou, X., and Gulari, E., *J. Catal.* **94,** 128 (1985).
63. Christman, K., and Ertl, G., *Surf. Sci.* **60,** 365 (1976).
64. Gasior, M., Gasior, I., and Grzybowska, B., *Appl. Catal.* **10,** 87 (1984).
65. Centi, G., and Trifiro, F., *Catal. Rev.–Sci. Eng.* **28,** 165 (1986).
66. Baiker, A., Dollenmeier, P., He, R., and Wokaun, A., *J. Catal.* **100,** 345 (1986).
67. Carballo, L. M., and Wolf, E. E., *J. Catal.* **53,** 366 (1978).
68. Otsuka, K., Hatano, M., and Morikawa, A., *J. Catal.* **79,** 493 (1983).